Kinetics of ion channel modulation by cAMP in rat hippocampal neurones

Barrie Lancaster[1], Hua Hu[2], Barry Gibb[1] and Johan F. Storm[2]

[1] *Wolfson Institute for Biomedical Research, University College London, Gower Street, London WC1E 6BT, UK*
[2] *Department of Physiology, Institute of Basal Medical Sciences, and Centre for Molecular Biology and Neuroscience, University of Oslo, PB 1103, Blindern, N-0317 Oslo, Norway*

Ion channel regulation by cyclic AMP and protein kinase A is a major effector mechanism for monoamine transmitters and neuromodulators in the CNS. Surprisingly, there is little information about the speed and kinetic limits of cAMP–PKA-dependent excitability changes in the brain. To explore these questions, we used flash photolysis of caged-cAMP (DMNB-cAMP) to provide high temporal resolution. The resultant free cAMP concentration was calculated from separate experiments in which this technique was used, in excised patches, to activate cAMP-sensitive cyclic nucleotide-gated (CNG) channels expressed in *Xenopus* oocytes. In hippocampal pyramidal neurones we studied the modulation of a potassium current (slow AHP current, I_{sAHP}) known to be targeted by multiple transmitter systems that use cAMP–PKA. Rapid cAMP elevation by flash photolysis of 200 μM DMNB-cAMP completely inhibited the K^+ current. The estimated yield (1.3–3%) suggests that photolysis of 200 μM caged precursor is sufficient for full PKA activation. By contrast, extended gradual photolysis of 200 μM DMNB-cAMP caused stable but only partial inhibition. The kinetics of rapid cAMP inhibition of the K^+ conductance (time constant 1.5–2 s) were mirrored by changes in firing patterns commencing within 500 ms of rapid cAMP elevation. Maximal increases in firing were short-lasting (< 60 s) and gave way to moderately enhanced levels of spiking. The results demonstrate how the fidelity of phasic monoamine signalling can be preserved by the cAMP–PKA pathway.

(Resubmitted 12 June 2006; accepted after revision 3 August 2006; first published online 10 August 2006)
Corresponding author B. Lancaster: Wolfson Institute for Biomedical Research, University College London, Gower Street, London WC1E 6BT, UK. Email: b.lancaster@ucl.ac.uk

Neuronal excitability changes induced by transmitters can take effect within milliseconds or several seconds. The speed of these changes depends on the steps between neurotransmitter receptor occupancy and changes in ion channel activity, usually due to changes in channel open probability. For the common ionotropic effects of transmitters such as acetylcholine, glutamate and GABA, the fast kinetics of the synaptic responses reflect tight coupling between ligand binding and ion channel opening. These transmitters also act via metabotropic receptors coupled to G proteins that, directly or via signalling cascades, modulate the gating of ion channels. The same evoked release of glutamate or GABA that produces a fast ionotropic response also generates slower, G protein-mediated, postsynaptic potentials with rise times of tens (Miller *et al.* 1995) to hundreds of milliseconds (Pfrieger *et al.* 1994; Batchelor & Garthwaite, 1997; Heuss *et al.* 1999). These metabotropic effects provide a slower, more flexible and modifiable link between receptor activation and neuronal excitability.

The kinetics of ion channel modulation by diffuse, non-synaptic metabotropic neurotransmitters – so called 'volume transmission' (Agnati *et al.* 1995; Zoli *et al.* 1999; Agnati & Fuxe, 2000;) – are difficult to assess independently of the dynamics of transmitter release and diffusion. This is partly because there are often no ionotropic receptors to provide instantaneous readout of the presence of agonist. Noradrenaline is one of the most widespread metabotropic transmitters in the brain where it is released by wide-ranging fibres from the locus coeruleus. The β-noradrenergic receptors activate adenylyl cyclase (AC) leading to elevation of cAMP and activation of protein kinase A (PKA). In cardiac myocytes, photorelease or rapid application of β agonists suggests a delay of 1.7–5 s between receptor stimulation and cAMP elevation, followed by a range of subsequent rates of ion channel modulation (Frace *et al.* 1993; Nakashima & Ono, 1994; Tanaka *et al.* 1996). Although ion channel modulation by the AC–cAMP–PKA cascade has been extensively studied in the mammalian CNS (see, e.g. Nicoll, 1988; Nicoll *et al.*

 DOI: 10.1113/jphysiol.2006.115295

1990; Hoffman & Johnston, 1998; Storm *et al.* 2000; Davare *et al.* 2001), the kinetics of this second messenger process in neurones is not well characterized.

In particular, the physiological rate of cAMP elevation in mammalian neurones remains unknown. By analogy with a diffusely acting neurotransmitter (noradrenaline), it might be assumed that rises in cAMP are gradual and prolonged, occurring throughout the cell. However, this intuitive view has been challenged by new evidence suggesting compartmentalization of cAMP signalling, allowing for transient and local regulation of cyclic nucleotide-gated channels (Rich *et al.* 2000, 2001) or PKA-dependent actions (Jurevičius & Fischmeister, 1996; Davare *et al.* 2001) within cAMP microdomains. To further our understanding of these two different modes of cAMP signalling we used photorelease of cAMP to test the effects of gradual, prolonged cAMP elevation *versus* rapid, transient cAMP elevation within single neurones.

To determine the time course of a prominent example of cAMP-dependent ion channel modulation, we have studied the slow afterhyperpolarization current (I_{sAHP}) in hippocampal pyramidal cells. This is an outward Ca^{2+}-activated K^+ current that follows depolarization-evoked Ca^{2+} influx. After brief Ca^{2+} influx or bursts of action potentials this current displays a distinct slow, rising phase followed by an even slower decay (Lancaster & Adams, 1986). I_{sAHP} has a well-defined sensitivity to β-adrenergic receptors and cAMP–PKA (Madison & Nicoll, 1986*b*; Pedarzani & Storm, 1993). The results, obtained by photorelease of cAMP, demonstrate distinctive actions of rapid and gradual changes in [cAMP], and reveal an unexpectedly dynamic regulation of ion channels and excitability by the cAMP–PKA pathway.

Methods

Hippocampi were obtained from 16- to 24-day-old rats after halothane anaesthesia or cervical dislocation followed by decapitation. These procedures were in accordance with the UK Animals (Scientific Procedures) Act 1986, or the Norwegian Ministry of Agriculture statute 1996. Transverse slices (300–400 μm) were cut using a Vibratome and slices transferred to an interface storage chamber. The bath solution contained (mM): 119 NaCl, 2.5 KCl, 1.3 $MgCl_2$, 1 NaH_2PO_4, 26 $NaHCO_3$, 2 $CaCl_2$ and 11 glucose, equilibrated with 95% O_2–5% CO_2 to pH 7.4. Chemicals were obtained from Sigma unless stated otherwise. The pipette solution was (mM): 150 potassium methylsulphate (ICN Biomedicals, or City Chemical), 10 Hepes, 10 KCl, 4 NaCl, 2–4 Mg_2ATP, 0.4 Na_4GTP. The solution was adjusted to 280–290 mosmol l^{-1}; pH 7.35–7.4. Osmolarity was adjusted with KCL and pH adjusted with KOH Additions to this solution were Rp-cAMPS (Biolog, Bremen, Germany); 4,5-dimethoxy-2-nitrobenzyl cAMP (DMNB-cAMP) and dibromo BAPTA (Molecular Probes). The A kinase anchoring protein (AKAP) inhibitor Ht31 was obtained from two different sources, in-house synthesis at University College London and a gift from Dr Kjetil Tasken, University of Oslo. The compound was dissolved in DMSO before dilution into the pipette solution at concentrations from 75 to 250 μM. Rapid cAMP release was performed using a Rapp flashlamp (Rapp OptoElectronic) with a 700 μm diameter quartz light guide attachment positioned over the recording area. Gradual photolysis of caged cAMP was accomplished using the xenon lamp of an upright microscope with the exposure duration controlled by a shutter (Zeiss). Whole-cell patch clamp recordings were performed on CA1 pyramidal cells at a temperature of 28–30°C unless stated otherwise. For voltage clamp recording, access resistance during recordings was < 25 MΩ and was compensated at least 60% using an Axopatch 1D or 200B (Molecular Devices). The slow AHP current was elicited with a conventional procedure comprising 80 ms depolarizing steps from -60 mV to -10 mV (0.05 Hz). These steps generate unclamped Ca^{2+} influx; upon stepping back to -60 mV, two main components of tail current can be observed. An early component which decays over a few hundred milliseconds largely comprises an apamin-sensitive small-conductance Ca^{2+}-activated K^+ (SK) current (Stocker *et al.* 1999); this is followed by the cAMP-sensitive I_{sAHP} which decays over seconds (Fig. 2*A*). Quantitative comparison of sAHP current after various manipulations used charge transfer during a 1 s epoch following the decay of other currents. The persistent current was normalized between the holding current (voltage clamped at -60 mV) at the onset of whole-cell recording and the maximum plateau value achieved in that cell. Current clamp recordings used an Axoclamp 2A amplifier. Data acquisition and analysis used pCLAMP (Molecular devices) and Origin (OriginLab Corp) software. Statistical significance was assessed by paired or unpaired Student's *t* test as appropriate.

Recombinant CNG channels; plasmid preparation and expression

The plasmid pXO2a, expressing the recombinant CNG channel X-fA4 (Young & Krougliak, 2004), was a kind gift from Edgar Young. The plasmid DNA was linearized with *Not*I prior to cleaning using the QIA quick PCR purification system (Qiagen). Pure, linear DNA was then used as template material in the T7 mMessage mMachine kit (Ambion) as per instructions. The resulting capped RNA was cleaned and isolated using the MEGAclear kit (Ambion) prior to concentration in the RNeasy MinElute Cleanup kit (Qiagen). This twofold strategy resulted in capped RNA that was both highly pure and concentrated. The capped RNA was finally quantified

on a NanoDrop ND-1000A spectrophotometer, prior to dilution to 500 ng ml^{-1} with RNase-free water, aliquoted and stored at −80°C.

Stage 5–6 oocytes were isolated from *Xenopus laevis* and injected with 25 ng of the capped RNA encoding the X-fA4 chimeric CNG channel. After 3–5 days the oocytes were stripped of the follicular layer and vitelline membrane. Recordings were then performed on excised membrane patches at room temperature. The bath solution was (mm): NaCl 115, Na_2EDTA 1, Na_4EGTA 5, Hepes 10, adjusted to pH 7.4. The pipette solution was identical except for the addition of 3 mm $MgCl_2$ (free concentration ∼1.4 mm). Inside-out patches were used to determine the cAMP sensitivity of the channels using bath application of cAMP (CalBiochem). The EC_{50} was obtained from a Hill equation fit to the concentration–response data. Outside-out patches were used for flash photolysis experiments in which 40 μm DMNB-cAMP was added to the pipette solution. For multiple flash exposures, the interval between flashes was 40–60 s which provided ample time for recharging the lamp capacitors. Other photolysis and electrophysiological methods were as described above.

Results

Estimating the concentration of photoreleased cAMP

As a functional assay for the concentration of cAMP produced from DMNB-cAMP, we used current through

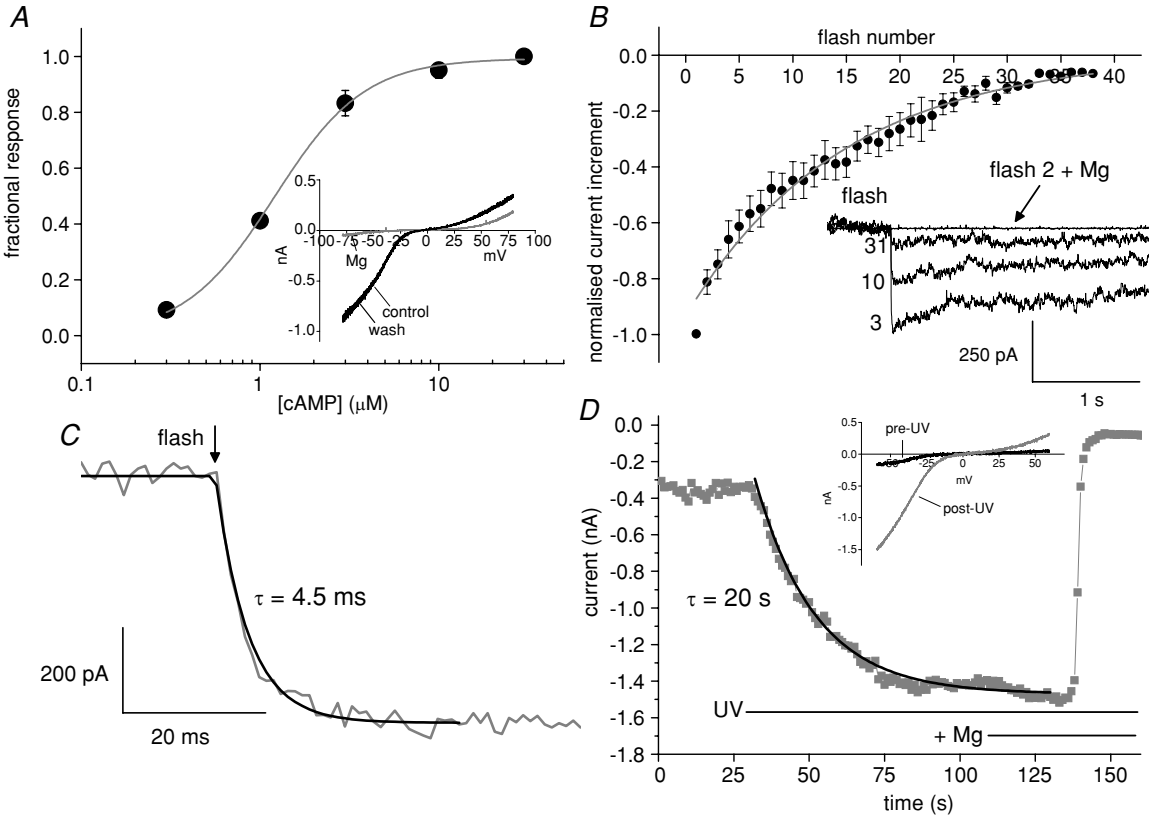

Figure 1. Calibration of flash responses as a cAMP concentration change
A, concentration–response curve for cAMP performed on inside-out patches from oocyte membrane containing CNG channels. Each point represents the mean ± S.E.M. of 4 patches from separate oocytes. The continuous line is a curve derived from the Hill equation. Half-maximal current activation was observed at a cAMP concentration of 1.2 μM. Inset, current–voltage plot for an outside-out membrane patch containing cAMP-sensitive CNG channels. The pipette contained 30 μM cAMP. The grey trace illustrates block when 3 mM Mg^{2+} was added to the external solution. *B*, amplitude of the CNG channel response to increasing numbers of UV flashes normalized to the first response (each point represents mean ± S.E.M. from 7 to 10 outside-out patches with 40 μM DMNB-cAMP in the recording pipette). The fitted exponential is a convenience to illustrate a detection limit of 30–40 flash responses. The inset superimposes individual traces for the 3rd, 10th and 31st UV flashes, holding potential −60 mV. No response was observed when Mg^{2+} was present during the second flash. *C*, flash photolysis of DMNB-cAMP activates CNG current (grey trace) within milliseconds following a flash (arrow). The black line shows a fit with a single exponential. *D*, photolysis of DMNB-cAMP using continuous illumination with the microscope UV source activates CNG current (grey symbols) over tens of seconds. Subsequent addition of 3 mM Mg^{2+} to the bath blocks the current as described above. The black line is a single exponential fit to the data.

modified cyclic nucleotide-gated (CNG) channels. These channels (termed X-fA4; Young & Krougliak, 2004) show a high sensitivity to cAMP. Excised patches obtained from *Xenopus* oocytes expressing these channels were used for the experiments. Concentration–response data obtained from inside-out patches show that the EC_{50} for activation by cAMP was 1.2 μM (Fig. 1*A*, $n = 4$). These CNG channels show a voltage-dependent block by Mg^{2+}. This property was used to confirm the identity of the current evoked by cAMP elevation. Figure 1*A* inset shows data from an outside-out patch exposed to a saturating concentration of cAMP (30 μM) in the patch pipette. Mg^{2+} in the recording pipette caused rectification by blocking outward current under control conditions. Bath application of 3 mM Mg^{2+} caused a reversible block which was more profound for the inward current as reported previously (Zagotta & Siegelbaum, 1996).

Outside-out patches with pipettes containing 40 μM DMNB-cAMP were used to test the response to photoreleased cAMP. The fractional photolysis per flash was estimated in two ways. Firstly, a series of UV exposures (40–60 s intervals) was performed until responses were no longer detectable, at which point the caged compound was effectively exhausted. Sample traces (Fig. 1*B* inset) illustrate the flash responses, which were blocked by external Mg^{2+}. The baselines have been normalized for convenience although in practice some current noise was observed before the flash responses, possibly due to agonist activity of the uncaged compound at the CNG channel.

Summary data for the current increment per flash (Fig. 1*B*, $n = 7$–10 patches per point) show that there were 30–40 detectable flash responses. The intersection (flash number 33) of the fitted curve with a conservative cut-off of 10% of maximal response suggests 3% photolysis per flash. In a subset of these experiments, there was a clear maximum patch current evoked by photorelease. In these cases, the fractional increase in basal CNG current over a number of flashes was converted to an increase in cAMP concentration using the concentration–response data for these channels (Fig. 1*A*). This calculated increment in [cAMP] then allowed a separate estimation of the percentage photolysis per flash of $1.3 \pm 0.3\%$. ($n = 4$). These values are likely to overestimate the photolysis that would occur in slices since there is no intervening tissue between the light guide and excised patches that otherwise would absorb UV.

The rise time of current in patches containing CNG channels following photorelease of cAMP approximates to the rate of rise of [cAMP]. For flash photolysis (Fig. 1*C*) the mean rise time constant was 7.5 ± 1.3 ms (range 2.0–20.2 ms, $n = 14$) at room temperature which is about 10^3 times faster than the rate of inhibition of the K^+ current in hippocampal neurones (Figs 3 and 5). In contrast, the microscope UV source caused a slow increase in CNG current (Fig. 1*D* inset shows the characteristic *I*–*V* relation) over tens of seconds until a plateau was reached (Fig. 1*D*). On the assumption that the plateau represents the maximum patch current, Mg^{2+} was then applied to separate CNG channel current from any leak (usually small). According to the concentration–response curve from inside-out patches we know that 1 μM cAMP causes 41% activation and 3 μM causes 83% activation. We then used the 41–83% rise time to estimate the rate of increase in [cAMP] within the patch. The average rate of rise was 68 ± 13 nM s^{-1} (8 patches). To compare with that, in four patches in which flash photolysis gave the maximum current on the first flash, the same estimation method indicates that flash photorelease caused [cAMP] to rise by 371 ± 125 nM ms^{-1}. This demonstrates that flash photolysis causes a very rapid increase in [cAMP] – more than 5000 times faster than the gradual elevation caused by the microscope UV source.

Photoreleased cAMP inhibits the sAHP current

Depolarization-evoked Ca^{2+} influx activates three distinct Ca^{2+}-dependent K^+ channel types in hippocampal pyramidal cells: BK, SK and sAHP channels (Madison & Nicoll, 1982; Lancaster & Adams, 1986; Storm, 1987; Lancaster & Nicoll, 1987; Stocker *et al.* 1999; Gu *et al.* 2005). Figure 2*A* shows typical tail currents following depolarization-induced Ca^{2+} influx in a CA1 pyramidal cell; there is an early tail current that is largely caused by SK channels (Stocker *et al.* 1999), followed by the slow AHP current (I_{sAHP}); the voltage-dependent BK channels close too fast to be visible in these records. The target of our investigation in this paper is I_{sAHP}, which is inhibited by multiple transmitters via cAMP–PKA (Madison & Nicoll, 1982, 1986*b*). Figure 2*A* and *B* shows that release of cAMP from a photolabile derivative (DMNB-cAMP within the pipette solution, 200 μM), caused reversible inhibition of I_{sAHP}.

When I_{sAHP} is activated intermittently by voltage-dependent Ca^{2+} influx, it is a transient current. This makes it difficult to resolve cAMP actions on a second or sub-second timescale. To achieve a stable, tonically active current, we used internal perfusion with dibromo BAPTA (DBB; Lancaster & Batchelor, 2000). This causes the development of a persistent K^+ current that shares all observed properties of I_{sAHP} (Lancaster & Batchelor, 2000). Like I_{sAHP}, the persistent current is voltage independent; it prevents or occludes the depolarization-evoked I_{sAHP}; and it is not observed in cells which lack I_{sAHP} such as some fast-spiking interneurones. The persistent current is also pharmacologically indistinguishable from I_{sAHP}. In particular, the two currents show the same sensitivity to noradrenaline and cAMP (Lancaster & Batchelor, 2000). In this study we therefore assume that the persistent K^+ current and I_{sAHP} are due to activity of the same

K^+ channels. Nevertheless we will refer to the dibromo BAPTA-induced current as the persistent K^+ current to distinguish it from I_{sAHP} evoked by depolarization.

Inhibition of the persistent K^+ current by photoreleased cAMP is illustrated in Fig. 2*C*. The large inward shift in the current used to clamp the cell close to resting potential (holding current) was accompanied by a decrease in slope conductance (Fig. 2*D*) with a null potential close to the calculated E_K of −110 mV. The time course of this effect is shown in Fig. 2*E*; the persistent K^+ current contribution to the holding current developed during the first 2 min and was rapidly inhibited by photoreleased cAMP. Recovery from inhibition appeared to be biphasic with a rapid phase of substantial recovery within 1 min followed by much slower recovery over > 5 min. We have not identified an explanation for this slow recovery. A persistent activation of PKA as reported in *Aplysia* sensory neurones (Muller & Carew, 1998) would account for this observation, although we do not know if this could occur on the timescale of our experiments.

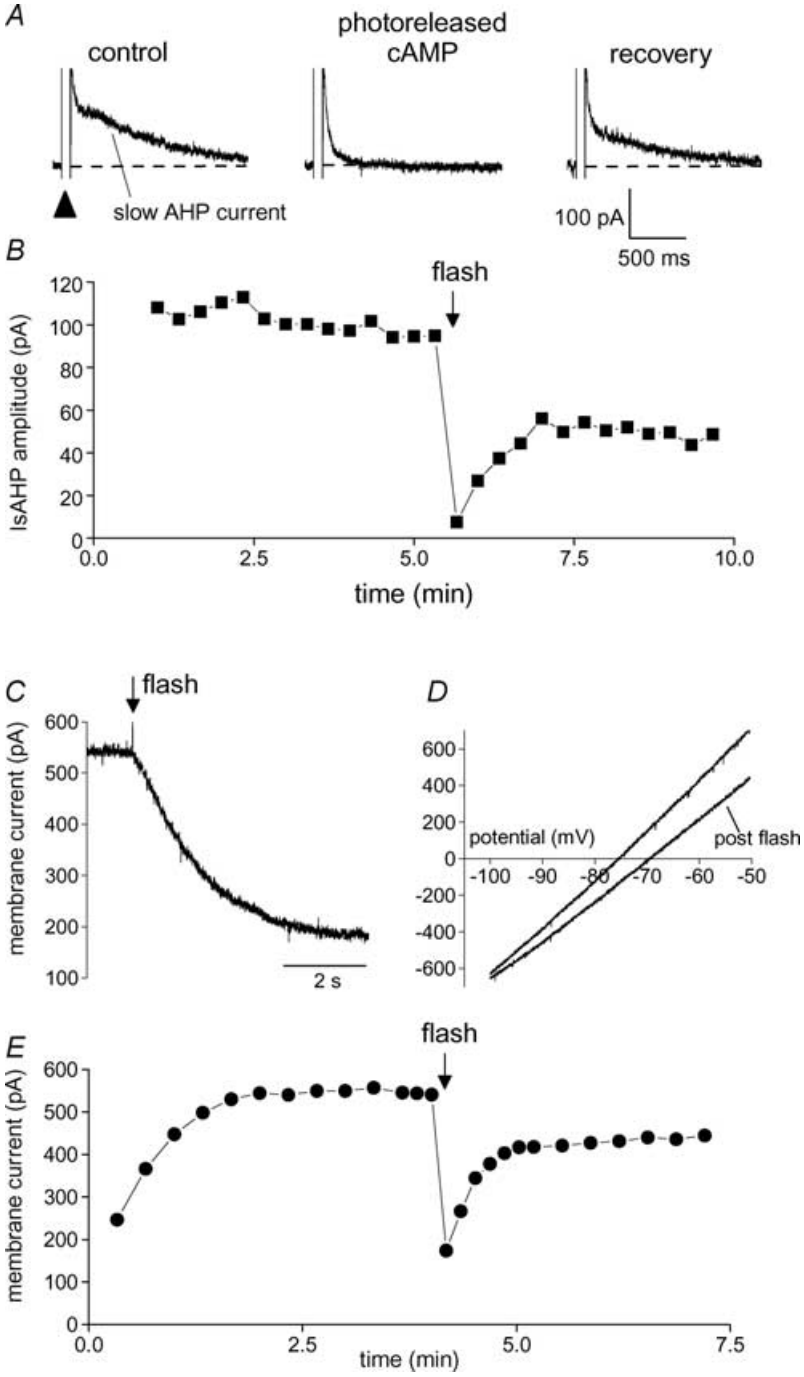

Figure 2. Photorelease of cAMP inhibits the slow AHP potassium conductance
A, a depolarizing step to generate Ca^{2+} influx (arrowhead) is followed by Ca^{2+}-dependent tail currents. The prominent slow component is the slow AHP current. Individual traces show I_{sAHP} (indicated) preceding (control), 5 s after photorelease of cAMP and 2.5 min after release of cAMP (recovery). *B*, time course of peak amplitude of I_{sAHP} shown in *A*. Photorelease of cAMP occurs at the flash (arrow). *C*, action of photoreleased cAMP on the persistent K^+ current; cAMP release inhibits the tonically active outward current, holding potential −60 mV. *D*, *I–V* plots generated by a 3 s voltage ramp from −100 to −50 mV. K^+ current inhibition (post flash trace) is associated with a decrease in conductance and shift in the zero current potential from −76 to −70 mV. *E*, time course of the experiment shown in *C* and *D*. Outward current develops as dibromo BAPTA diffuses from the pipette into the cell. Current inhibition and recovery follows the release of cAMP (flash).

The actions of photoreleased cAMP are identical in the presence of 1–2 mM external Cs^+ ($n = 5$, data not shown) which blocks the cyclic nucleotide-sensitive cation current I_h (Halliwell & Adams, 1982). In the absence of dibromo BAPTA, the effect of photoreleased cAMP on the holding current at −60 mV (−21 ± 4 pA, $n = 8$) or −85 mV (−25 ± 6 pA, $n = 5$) was very small; these values are not significantly different from those obtained with UV exposure alone (−19 ± 4 pA, $n = 4$; see Fig. 5; $P = 0.78$ and 0.44, respectively, by independent Student's t test). This shows that the action of cAMP on holding current required the presence of the persistent K^+ current and that actions on I_h did not contribute to the results. The cyclic nucleotide binding site of CNG channels can be bound by the 8 bromo and 8 cPT derivatives (Hagen *et al.* 1996; Savchenko *et al.* 1997) as well as DMNB-cAMP (Fig. 1). Since HCN and CNG channels have similar cyclic nucleotide binding sites (Santoro *et al.* 1997; Ludwig *et al.* 1998), a plausible explanation for there being no response of I_h in our experiments is that unphotolysed DMNB-cAMP acted as a ligand at the cyclic nucleotide binding site of HCN channels and thereby obscured any further action of released cAMP.

Elevation of cAMP is the initial step in the PKA transduction pathway – well characterized as the mechanism for I_{sAHP} inhibition by monoamines (Madison & Nicoll, 1986*a*; Pedarzani & Storm, 1993). If the kinetics of inhibition reflects kinase activity, the onset of inhibition following cAMP release is expected to be highly temperature sensitive. The temporal resolution of cAMP action required to test this possibility was obtained by exposing the persistent K^+ current to photoreleased cAMP (Fig. 3). The onset of inhibition showed pronounced temperature dependence. The sample traces in Fig. 3*A* show the inhibition (inward current) following flash-evoked cAMP release at 21°C (normalized to the 30°C trace) or 30°C together with single exponential fits. The inset is a comparison of the pooled time constants from similar data: 6.4 ± 0.7 s at 21°C ($n = 6$) *versus* 1.9 ± 0.2 s at 30°C ($n = 10$). The plots in Fig. 3*B* show summary data for first few seconds of inhibition. Assuming linear temperature dependence (likely to be an underestimate for enzyme activity), the time constant for inhibition at 37°C will be about 600 ms. These data demonstrate that the rate of K^+ current inhibition following cAMP elevation is 3- to 4-fold faster at 30°C than 21°C. This high temperature sensitivity is consistent with an enzymatic mechanism.

The specific involvement of PKA was tested using Rp-cAMPS, which is a competitive inhibitor of PKA at the cAMP binding site. We found that the effect of photoreleased cAMP on the depolarization-evoked I_{sAHP} was prevented in a concentration-dependent fashion after adding Rp-cAMPS to the intracellular medium of the recording pipette (Fig. 3*C*). The kinetics of recovery from inhibition was not studied in detail. The recovery presumably results from the phosphatase activity that has been demonstrated in these cells (Pedarzani *et al.* 1998) and the temperature dependence (Fig. 3*D*) is consistent with this hypothesis. The initial rapid phase of recovery still occurred even when I_{sAHP} was not evoked for 3 min after photolysis (Fig. 4*B*, filled circles). This has two implications. Firstly, recovery is not state dependent because it is the same whether or not the current/channels is/are active. Second, the phosphatases presumed responsible for recovery are not dependent on the elevated calcium that accompanies repetitive activation of the I_{sAHP}; this is corroborated by the similar recovery of the persistent current (Fig. 2*D*).

Distinct actions of rapid *versus* gradual photorelease of cAMP

The rapid photorelease of caged cAMP in Figs 2 and 3 was achieved using flash photolysis, a UV exposure of ≤ 1 ms. Flash photolysis of 200 μM caged cAMP produced almost complete inhibition of the persistent K^+ current as well as I_{sAHP}, a result that was observed across separate series of experiments (Figs 3*D*, and 4*B* and *C*). In contrast, to the results obtained with rapid cAMP release, we found that there was a limit to the inhibition caused by more gradual photorelease of caged cAMP. This partial effect is illustrated by the traces in Fig. 4*C*, which compare the maximal effects of rapid and gradual photolysis. The action of slow cAMP release might result from a lower free cAMP level. For example, rapid photorelease from low levels (40 μM) of caged cAMP caused only 43% inhibition of I_{sAHP} (Fig. 4*B* filled squares, $n = 5$).

Summary data comparing inhibition of I_{sAHP} under three experimental conditions are shown in Fig. 4*C*. I_{sAHP} was significantly reduced by 30 s of UV exposure in cells recorded with 200 μM caged cAMP in the electrode (grey circles, pre-UV 61 ± 4 pC, 30 s UV 27 ± 5 pC; $P < 0.001$, paired t test, $n = 6$). UV exposure alone had no effect (open circles, pre-UV 58 ± 8 pC, 30 s UV 56 ± 9 pC; $P = 0.14$, paired t test, $n = 6$). The filled circles show the almost complete inhibition of I_{sAHP} by flash photolysis of 200 μM caged cAMP (pre-UV 56 ± 6 pC, post-UV 2 ± 3 pC; $P < 0.001$, paired t test, $n = 6$).

Subsequently, in order to determine the action of gradual cAMP release in more detail we tested this on the persistent K^+ current. Continuous release of cAMP caused a clear but only partial inhibition, revealed when the K^+ current settled at a new steady-state value (Fig. 4*D*1); recovery then commenced promptly at the end of UV illumination. To test directly that the caged cAMP was not exhausted by the continuous UV illumination, flash photolysis was superimposed on the steady-state level. In all 12 cells tested, a UV flash caused further inhibition

of K^+ current (Fig. 4*D*2), indicating that a reservoir of unphotolysed DMNB-cAMP was present. Instead of depletion, we interpret the steady-state condition as a point where cAMP release is sufficient to bring PKA and phosphatase activity into equilibrium. Thus, as soon as cAMP release decreased, phosphatase activity became predominant and allowed recovery of the current. The summary data from these experiments are plotted in Fig. 4*E*, in which the 30 s UV exposure is marked by the shaded area. The expanded timescale (inset Fig. 4*E*) shows that inhibition becomes apparent after 1.5–2 s of UV exposure. This is much slower than observed for flash photolysis (Figs 2 and 3) and is consistent with the much slower rate of cAMP accumulation defined earlier (Fig. 1). Photolysis for 5 s produced 29% inhibition of the persistent current ($n = 5$, data not shown); however, after 30 s photolysis the inhibition had reached an equilibrium value of only 44% (Fig. 4*E*). The effects of rapid photorelease of cAMP cannot therefore simply be mimicked by the cumulative effect of gradual release over longer periods.

Localization and specificity of cAMP–PKA signalling is partly determined by proximity of the kinase to the phosphorylation target. The association of PKA with a target occurs through A kinase anchoring proteins (AKAPs; reviewed in Colledge & Scott, 1999). These proteins are known to be required for PKA-mediated modulation of ion channels (Westphal *et al.* 1999)

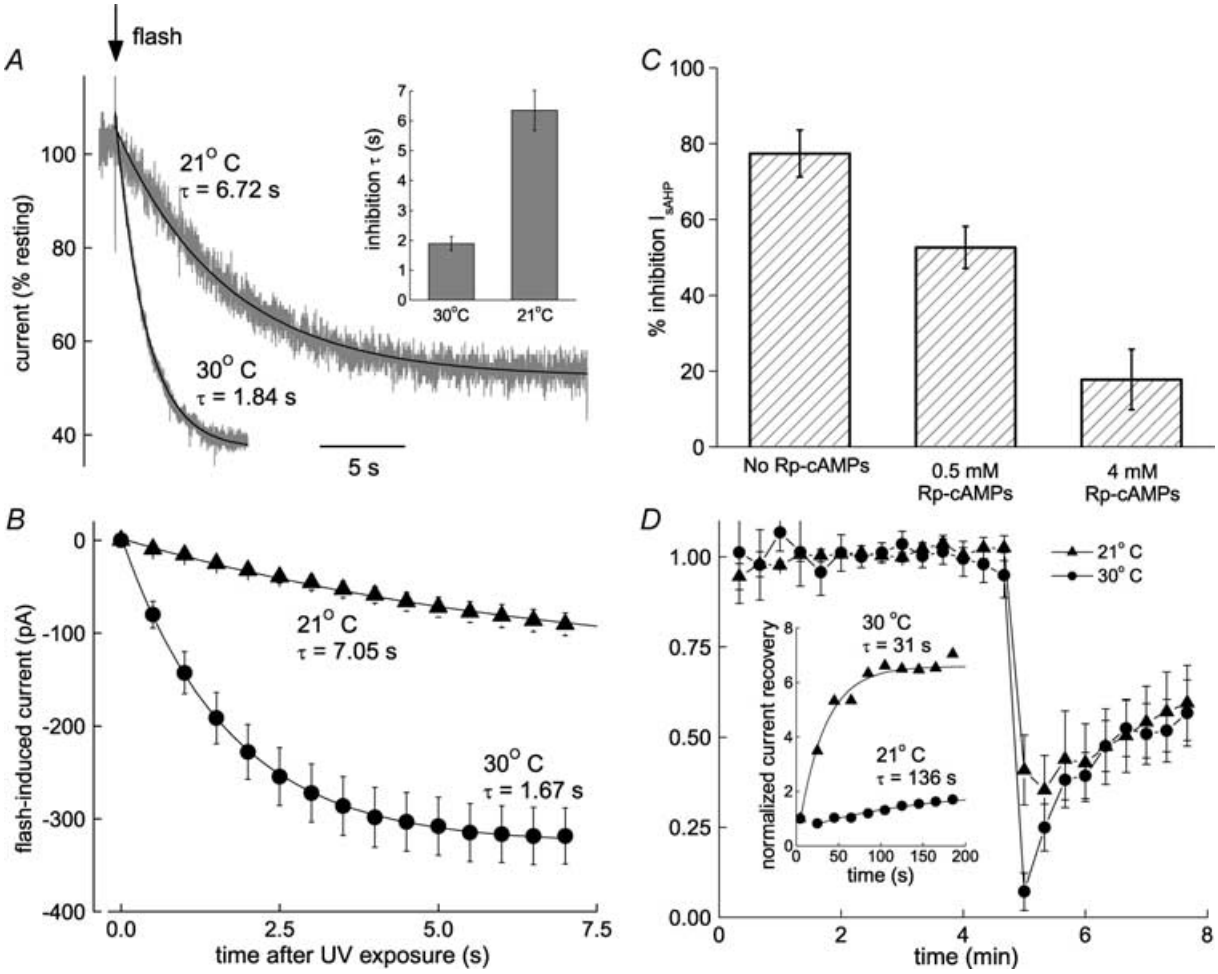

Figure 3. Protein kinase is required for cAMP action
A, the rate of persistent K^+ current inhibition following cAMP release has high temperature sensitivity. Sample traces at 21 and 30°C have been normalized and fitted with single exponentials. The histogram (inset) summarizes the time constants at 30°C (1.89 ± 0.24 s, $n = 10$) and 21°C (6.35 ± 0.66 s, $n = 7$). *B*, initial rates of inhibition at 21 and 30°C. The symbols show mean values (± S.E.M.) of inward current at 500 ms intervals (21°C, $n = 6$; 30°C, $n = 10$) following photolysis of the caged cAMP. The lines are single exponential fits to this data with time constants of 7.05 s at 21°C (fit executed over 20 s) and 1.67 s at 30°C (fit executed over 7 s). *C*, inhibition of I_{sAHP} by photoreleased cAMP (77 ± 6% control, $n = 5$) was attenuated by a PKA inhibitor to 53 ± 6% at 0.5 mM Rp-cAMPs ($n = 5$) and 18 ± 8% at 4 mM Rp-cAMPs ($n = 4$). *D*, inhibition and recovery of I_{sAHP} at 21°C ($n = 5$) and 30°C ($n = 4$). Initial recovery rates are temperature dependent (inset).

including cAMP-dependent modulation of cardiac Ca^{2+} current (Zhong *et al.* 1999). In hippocampal cells, the AKAP inhibitor peptide Ht31 (Carr *et al.* 1992) suppressed cAMP-dependent regulation of Na^+ current (Cantrell *et al.* 1999). In our hands, Ht31 had no apparent effect on the inhibition of I_{sAHP} by noradrenaline, isoprenaline or photoreleased cAMP. Thus, in 10 cells where Ht31 was applied intracellularly by adding it (75–250 μM Ht31) to the pipette solution, activation of the cAMP–PKA cascade still suppressed I_{sAHP}, rapidly and completely. In these experiments, the effects of noradrenaline (10 μM; $n = 2$), isoprenaline (100 nM–2 μM; $n = 4$) or photoreleased cAMP ($n = 4$) observed in Ht31-loaded cells were indistinguishable from the complete inhibition seen in control cells that were recorded without Ht31 in the pipette ($n = 50$), or in a cell filled with an inactive analogue of Ht31 (Ht31P; 50 μM; $n = 1$). The Ht31, which was found to be ineffective against isoprenaline, had been previously confirmed as a PKA anchoring disruptor (Carr *et al.* 1991) tested by PKA regulatory subunit-overlay *versus* AKAP95 (personal communication, Dr Kjetil Tasken, University of Oslo).

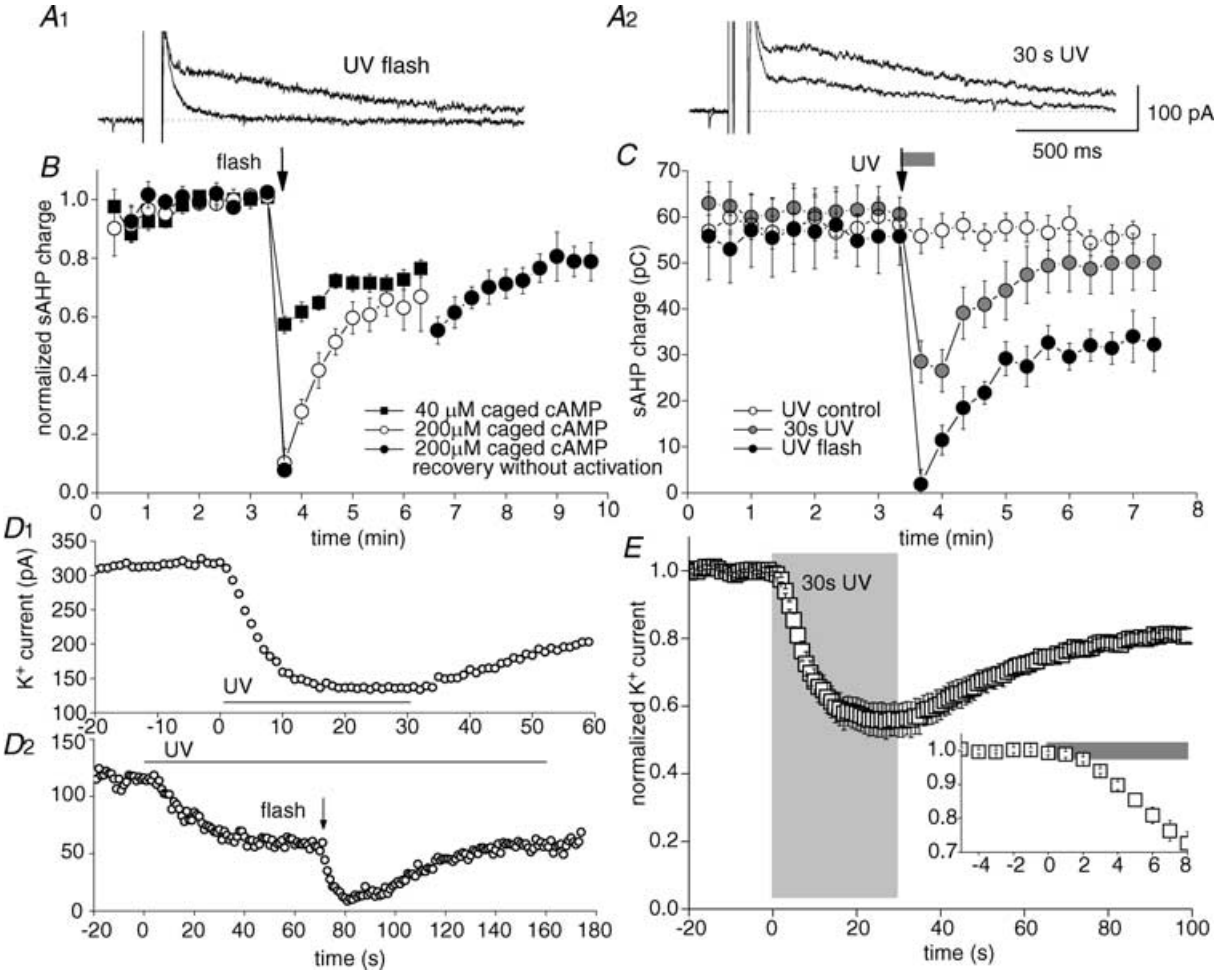

Figure 4. Actions of rapid *versus* gradual cAMP release
A, individual traces show I_{sAHP} before and after rapid (UV flash, *A*1) or gradual (30 s UV, *A*2) cAMP release. *B*, inhibition of I_{sAHP} by photolysis (arrow) of 40 μM (■) or 200 μM caged cAMP (circles); $n = 5$ for each condition. Charge transfer was measured during a 1 s epoch which commenced 500 ms after the depolarizing step to permit complete decay of other tail currents. *C*, comparison of I_{sAHP} inhibition by flash (arrow, black symbols, $n = 6$) or 30 s UV (grey bar, grey symbols, $n = 4$) exposure of 200 μM caged cAMP. Exposure to UV in the absence of caged cAMP is denoted by ○ ($n = 6$). *D*, slow release of cAMP during UV illumination caused a gradual inhibition of the persistent K^+ current which levelled off before complete inhibition was reached. *D*1, recovery from inhibition commenced when photolysis ceased. *D*2, after a stable level of inhibition was achieved with constant UV illumination, additional inhibition could be generated by rapid release of cAMP with flash photolysis (arrow). *E*, summary data for the action of slow cAMP accumulation on the persistent K^+ current ($n = 5$). Onset detail is shown in the inset graph. Grey rectangles indicate UV exposure.

Kinetic limits of K^+ current inhibition

To test the limits of cAMP–PKA-dependent ion channel inhibition, we tested the effect on the persistent K^+ current of photorelease from three (40–1000 μM) caged cAMP concentrations. Since photolysis reaction efficiency is independent of the ester concentration (Nerbonne *et al.* 1984), this concentration range (25-fold) should be reflected in the range of photoreleased cAMP. In each case the same UV discharge was directed to the slice using a 700 μm fibre-optic light guide adjacent to the submerged surface of the tissue. This avoided reflection and scattering by the overlying solution, leaving the concentration of caged compound as the major variable in the pooled data of Fig. 5.

The data traces in Fig. 5*A* are averages for each caged cAMP concentration ($n = 5$) and control data ($n = 4$). The inward current beginning at the UV flash represents inhibition of persistent K^+ current after photorelease of cAMP from different concentrations of caged compound compared with the control condition (no caged cAMP). For the 200 μM and 1 mM data, the start of recovery from inhibition can be detected towards the end of the traces. The smooth lines are single exponential fits which originate 1 s after the flash and describe satisfactorily most of the current decay, although when extrapolated back to time zero (Fig. 5*B*) they overestimate the rate of inhibition during the first 500 ms. This S-shaped onset could result from cooperative activation of PKA. The summary data for inhibition time constants and amplitude of inhibition are shown in Fig. 5*C* and *D*, respectively. The rate of inhibition is much faster for the 5-fold increase in caged cAMP, from 40 to 200 μM (4229 ± 638 to 2213 ± 183 ms, $P = 0.016$, unpaired *t* test, Fig. 5*C*). The

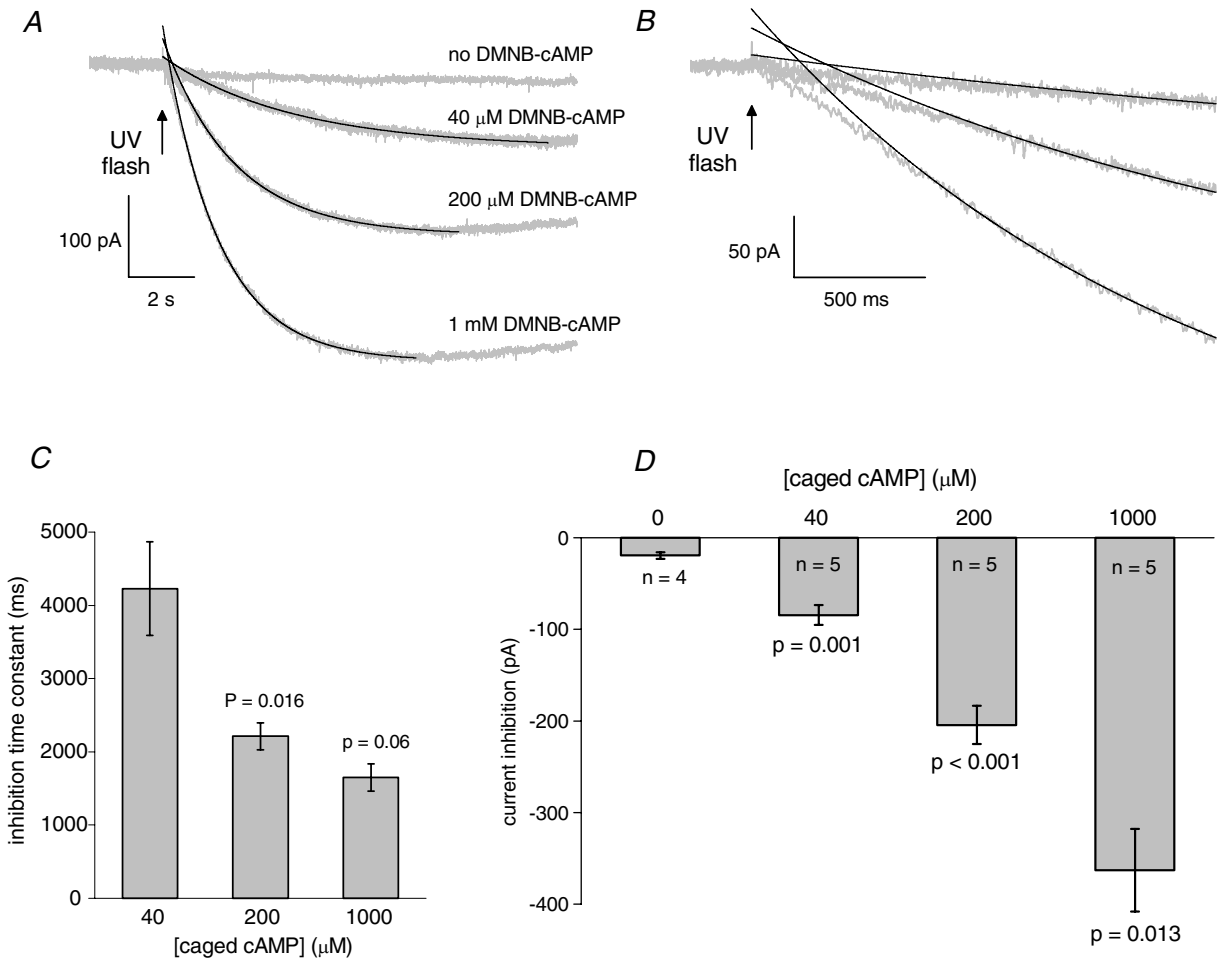

Figure 5. The kinetics of K^+ current inhibition by rapid release of cAMP
A, membrane current responses (grey) and single exponential fits (black) to a UV flash in the presence of different concentrations of caged cAMP, or no caged cAMP. *B*, expansions of the traces in *A* to show the delay in predicted inhibition observed at all caged cAMP concentrations. *C*, pooled data ($n = 5$) for the inhibition time constants at different caged cAMP concentrations as follows: 4.2 ± 0.6 s (40 μM); 2.2 ± 0.2 s (200 μM); 1.7 ± 0.2 s (1000 μM). *D*, peak current inhibition following the release of increasing concentrations of cAMP. In the absence of caged cAMP a small flash artefact is present.

time constant of inhibition after release from 1000 μM (1650 ± 186 ms) is not significantly faster than for 200 μM ($P = 0.06$, unpaired t test). This suggests that this time constant of 1650 ms is approaching the kinetic limit under these conditions. Each step increase in caged cAMP concentration produces significantly greater K^+ current inhibition following flash photolysis (Fig. 5*D*).

Changes in spike activity following release of cAMP

To determine the latency and extent of the excitability changes induced by the activity of the cAMP–PKA pathway, we tested the effect of cAMP photorelease on the firing properties of hippocampal pyramidal cells. The experiment consisted of four stages, starting with 1 s current injections to produce low frequency spiking (Fig. 6*A*, no prepulse). The average spike rate was 10 ± 0.8 Hz ($n = 6$, Fig. 6*D*) with a short latency to the first action potential < 100 ms (Fig. 6*C*). When a burst of spikes sufficient to produce a slow AHP preceded the 1 s pulse (Fig. 6*A*, + prepulse), the spike frequency was strongly reduced (1.5 ± 0.7 Hz, Fig. 6*B* and *D*) and the first spike latency increased to 800–900 ms (Fig. 6*C*). The individual trace during photorelease of cAMP (100 ms after the onset of the long pulse) is denoted by the open symbols in Fig. 6*B* and *C*; in this cell the increase in excitability is apparent about 400 ms after photorelease of cAMP. The latency of the first action potential decreased from 710 ± 80 ms before cAMP release to 450 ± 60 ms in the trace immediately after release ($P = 0.01$, paired

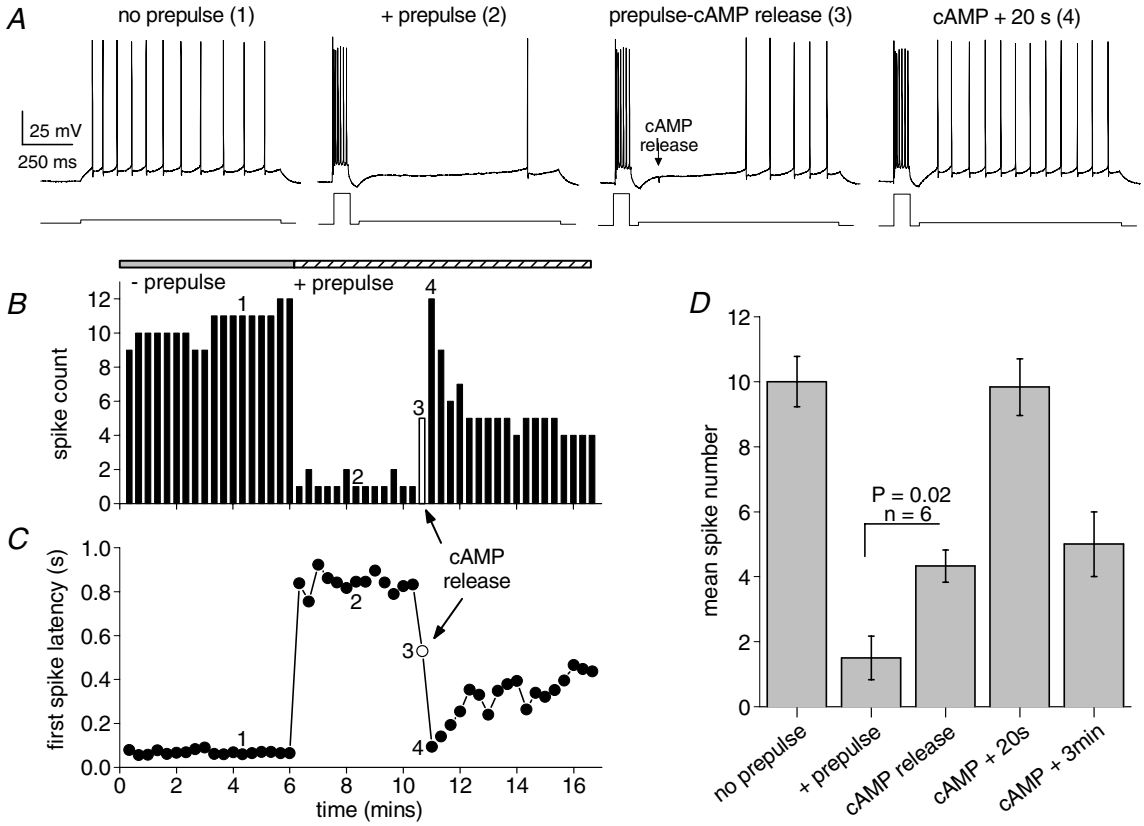

Figure 6. The kinetics of cellular excitability changes following rapid release of cAMP
A, the four panels show, from left to right, spike pattern during mild depolarization from a membrane potential of −63 mV (no prepulse); inhibition of firing by sAHP (+ prepulse); relief of inhibition immediately following cAMP release (prepulse-cAMP release); complete block of inhibition 20 s after cAMP release (cAMP + 20 s). The numbers for each trace refer to the time points indicated in *B* and *C*. *B*, spike count during the 1 s depolarizations of the experiment shown in *A*. Addition of the prepulse to evoke a slow AHP dramatically reduced spike numbers. The open bar denotes the point of photorelease of cAMP. The return to control excitability (4) representing complete suppression of the slow AHP is short-lasting. *C*, first spike latency during the 1 s depolarizations of the experiment in *A*. The slow AHP retards spiking until the release of cAMP (open symbol). *D*, pooled data (mean ± S.E.M.) for 6 experiments using the protocol in *A*. Mild depolarization evoked 10 ± 0.8 spikes which was reduced to 1.5 ± 0.7 spikes in the presence of a prepulse to generate sAHP. Significantly increased spiking (4.3 ± 0.5) was observed immediately after cAMP release and after 20 s excitability was indistinguishable from control activity (9.8 ± 0.9 spikes). Partial relief of cAMP action was seen after 3 min (5 ± 1 spike).

t test, $n = 6$). The pooled data (Fig. 6*D*, cAMP release) is a measure of cell spiking within a 900 ms epoch after cAMP elevation; this demonstrates a significant increase in excitability in less than 1s. Subsequently (cAMP + 20 s), there is a brief peak in spike number which relaxes to a more prolonged intermediate level of excitability (cAMP + 3 min, 5 ± 1 Hz, Fig. 6*B* and *D*). These data suggest that activation of the cAMP–PKA pathway is capable enhancing neuronal responsiveness within 500 ms of cAMP elevation.

Discussion

This study describes the kinetics of a form of ion channel modulation by the cAMP–PKA pathway in neurones after concentration jumps of cAMP generated by flash photolysis. Inhibition of the sAHP-like persistent K^+ conductance by this mechanism showed a time to peak of 6–7 s with time constants as short as 1.6 s and an S-shaped onset preceded by a slight delay. Elevation of [cAMP] caused concentration-dependent inhibition of I_{sAHP} that showed initial rapid recovery followed by a period of slower recovery. This was mirrored by changes in firing, detectable within 0.5–1 s of [cAMP] elevation.

How does the speed of ion channel modulation via cAMP–PKA compare with transduction mechanisms by membrane-delimited second messengers? The fastest G protein-coupled response on record had a rise time of < 30 ms (Miller *et al.* 1995). More typical are time constants in the 200–300 ms range, as for the muscarinic activation of GIRK channels (Nargeot *et al.* 1982), $GABA_B$-mediated inhibition of Ca^{2+} currents (Pfrieger *et al.* 1994) and synaptic responses generated by mGluRs (Batchelor & Garthwaite, 1997; Heuss *et al.* 1999). At the slower end of this scale, G protein-dependent actions on Ca^{2+} current in sympathetic neurones have time constants from 0.4 to 1.2 s (Zhou *et al.* 1997). The kinetics of ion channel modulation by cAMP–PKA are documented most extensively in cardiac myocytes where Ca^{2+} current requires 10–20 s for peak enhancement following cAMP concentration jumps (Richard *et al.* 1985; Frace *et al.* 1993; Tanaka *et al.* 1996). However, in the same cells the cAMP–PKA-dependent Cl^- current is activated with concentration-dependent time constants in the range 0.8–2.4 s (Nakashima & Ono, 1994). These values are very similar to our observations and suggest a transduction mechanism around 3–5 times slower than typically reported for neuronal G protein-coupled receptors.

Our estimate of a photolysis rate of 1.3–3% per flash is similar to other estimates using flashlamp-based systems (Nerbonne *et al.* 1984; Frace *et al.* 1993). At 40 μM DMNB-cAMP, these values predict 0.52 μM and 1.2 μM free cAMP, respectively. For a given flash intensity we assume that the fraction of photolysis in excised patches will be less than in a brain slice where tissue absorbance will attenuate the UV intensity. The level of resting cAMP in neurones is about 50 nM (Backsai *et al.* 1993) whereas maximal PKA activation requires [cAMP] in the 0.5–2 μM range (Hofmann *et al.* 1975). Since photolysis of 40 μM DMNB-cAMP only gave partial inhibition of I_{sAHP} in slices, this suggests less than full PKA activation in these experiments. Hence, our data are consistent with 0.5 μM or less cAMP produced by photolysis of 40 μM caged compound, i.e. 1.25% photolysis.

The time course of [cAMP] elevation following flash photolysis of 40 μM DMNB-cAMP was measured by using membrane patches containing a chimeric CNG channel with an appropriate cAMP sensitivity (EC_{50} 1.2 μM) for the range that activates PKA. The flash-induced rise in [cAMP] as detected by channel activity ($\tau = 7.5$ ms at room temperature) is comparable to the kinetics of rod CNG channels after photolysis of the DMNB ester of cGMP (Karpen *et al.* 1988). Thus, assuming a similar time course of [cAMP] elevation in the slice as in membrane patches, the rate of K^+ current modulation (Fig. 2) was about 10^3 times slower than the rise in cyclic nucleotide levels.

The initial rate of ion channel inhibition showed a slight delay or S-shape. Since this was observed over all concentrations of caged cAMP tested, it seems unlikely that hindered diffusion of cAMP caused the delay. However, the cooperative binding of four cAMP molecules required to activate PKA (Øgreid & Døskeland, 1981) would be consistent with an S-shaped rise time. Equally plausible, intermediate reaction steps leading to ion channel modulation may contribute to the observed delay. In hippocampal neurones, dopamine modulation of sodium current is sensitive to AKAP inhibition by Ht31, indicating that AKAPs link PKA to its substrate (Cantrell *et al.* 1999). If the K^+ current modulation by cAMP depends on a similar AKAP-mediated co-localization of PKA and substrate, this would be expected to facilitate rapid modulation. However, we found that the AKAP inhibitor peptide Ht31 did not affect the modulation of the K^+ conductance in CA1 pyramidal cells. This observation is consistent with the finding that PKA-dependent suppression of the slow AHP by noradrenaline in these cells is mediated by β1 adrenergic agonists (Madison & Nicoll, 1986*a*) which, in heart, appear to lack AKAP interaction (Kapiloff, 2002).

Monoamine transmission shows phasic (fast) and tonic (slow) characteristics which reflect firing patterns of monoaminergic neurones (Aston-Jones & Bloom, 1981), release kinetics and uptake (Cragg *et al.* 2003). How does the cAMP–PKA system preserve the distinction between fast and slow transmitter signals? It has been proposed that tonic PDE activity acts as a barrier for cAMP diffusion (Rich *et al.* 2001; Jurevičius *et al.* 2003; Barnes *et al.* 2005) and permits compartmentalization of cAMP signals. The

formation of microdomains of high [cAMP] allows for localized effects where maximal activation of PKA could occur in < 1 s (Rich *et al.* 2000; Zaccolo & Pozzan, 2002). We found that photolysis of 200 μM caged cAMP had the capacity to cause complete inhibition of the $I_{sAHP,}$ but the extent of inhibition was significantly greater for rapid than for gradual photorelease. This suggests that the capacity for ion channel modulation in neurones differs according to the rate of [cAMP] elevation. Faster and larger rises in [cAMP] arise from rapidly increasing and higher transmitter concentrations (Backsai *et al.* 1993), which would be expected from phasic monoamine signalling (Suaud-Chagny *et al.* 1995). Thus, the resulting production of rapid and large [cAMP] transients, possibly within microdomains, will result in faster modulation of channels (Nakashima & Ono, 1994; this paper), and thereby preserve the integrity of the fast signals arising as phasic discharge in monoaminergic neurones.

References

Agnati LF, Bjelke B & Fuxe K (1995). Volume versus wiring transmission in the brain: a new theoretical frame for neuropsychopharmacology. *Med Res Rev* **15**, 33–45.

Agnati LF & Fuxe K (2000). Volume transmission as a key feature of information handling in the central nervous system possible new interpretative value of the Turing's B-type machine. *Prog Brain Res* **125**, 3–19.

Aston-Jones G & Bloom FE (1981). Norepinephrine-containing locus coeruleus neurones in behaving rats exhibit pronounced responses to non-noxious environmental stimuli. *J Neurosci* **1**, 887–900.

Backsai BJ, Hochner B, Mahaut-Smith M, Adams SR, Kaang B-K, Kandel ER & Tsien RY (1993). Spatially resolved dynamics of cAMP and protein kinase A subunits in *Aplysia* sensory neurons. *Science* **260**, 222–226.

Barnes AP, Livera G, Huang P, Sun C, O'Neal WK, Cont M, Stutts MJ & Milgram SL (2005). Phosphodiesterase 4D forms a cAMP diffusion barrier at the apical membrane of the airway epithelium. *J Biol Chem* **280**, 7997–8003.

Batchelor AM & Garthwaite J (1997). Frequency detection and temporally dispersed synaptic signal association through a metabotropic glutamate receptor pathway. *Nature* **385**, 74–77.

Cantrell AR, Tibbs VC, Westenbroek RE, Scheuer T & Catterall WA (1999). Dopaminergic modulation of voltage-gated Na^+ current in rat hippocampal neurons requires anchoring of cAMP-dependent protein kinase. *J Neurosci* **19**, RC21.

Carr DW, Hausken ZE, Fraser ID, Stofko-Hahn RE & Scott JD (1992). Association of the type II cAMP-dependent protein kinase with a human thyroid RII-anchoring protein. Cloning and characterization of the RII binding domain. *J Biol Chem* **267**, 13376–13382.

Carr DW, Stofko-Hahn RE, Fraser ID, Bishop SM, Acott TS, Brennan RG & Scott JD (1991). Interaction of the regulatory subunit (RII) of cAMP-dependent protein kinase with RII-anchoring proteins occurs through an amphipathic helix binding motif. *J Biol Chem* **266**, 14188–14192.

Colledge M & Scott JD (1999). AKAPs: from structure to function. *Trends Cell Biol* **9**, 216–221.

Cragg SJ (2003). Variable dopamine release probability and short-term plasticity between functional domains of the primate striatum. *J Neurosci* **23**, 4378–4385.

Davare MA, Avdonin V, Hall DD, Peden EM, Burette A, Weinberg RJ, Horn MC, Hoshi T & Hell JW (2001). A β_2 adrenergic receptor signaling complex assembled with the Ca^{2+} channel Ca_v 1.2. *Science* **293**, 98–101.

Frace AM, Méry P-F, Fischmeister R & Hartzell HC (1993). Rate-limiting steps in the β-adrenergic stimulation of cardiac calcium current. *J Gen Physiol* **101**, 337–353.

Gu N, Vervaeke K, Hu H & Storm JF (2005). Kv7/KCNQ/M and HCN/h, but not KCA2/SK channels contribute to the somatic medium after-hyperpolarization and excitability control in CA1 hippocampal pyramidal cells. *J Physiol* **566**, 689–715.

Hagen V, Dzeja C, Frings S, Bendig J, Krause E & Kaupp UB (1996). Caged compounds of hydrolysis-resistant analogues of cAMP and cGMP: synthesis and application to cyclic nucleotide-gated channels. *Biochemistry* **35**, 7762–7771.

Halliwell JV & Adams PR (1982). Voltage-clamp analysis of muscarinic excitation in hippocampal neurons. *Brain Res* **250**, 71–92.

Heuss C, Scanziani M, Gähwiler BH & Gerber U (1999). G-protein-independent signaling mediated by metabotropic glutamate receptors. *Nat Neurosci* **2**, 1070–1077.

Hoffman DH & Johnston D (1998). Down regulation of transient K^+ channels in dendrites of hippocampal CA1 pyramidal neurons by activation of PKA and PKC. *J Neurosci* **18**, 3521–3528.

Hofmann F, Beavo JA, Bechtel PJ & Krebs EG (1975). Comparison of adenosine 3′: 5′-monophosphate-dependent protein kinases from rabbit skeletal and bovine heart muscle. *J Biol Chem* **250**, 7795–7801.

Jurevičius J & Fischmeister R (1996). cAMP compartmentation is responsible for a local activation of cardiac Ca^{2+} channels by β-adrenergic agonists. *Proc Natl Acad Sci U S A* **93**, 295–299.

Jurevičius J, Skeberdis VA & Fischmeister R (2003). Role of cyclic nucleotide phosphodiesterase isoforms in cAMP compartmentation following β_2-adrenergic stimulation of $I_{Ca,L}$ in frog ventricular myocytes. *J Physiol* **551**, 239–252.

Kapiloff MS (2002). Contributions of protein kinase A anchoring proteins to compartmentation of cAMP signaling in the heart. *Mol Pharmacol* **62**, 193–199.

Karpen JW, Zimmerman AL, Stryer L & Baylor DA (1988). Gating kinetics of the cyclic-GMP-activated channel of retinal rods: flash photolysis and voltage jump studies. *Proc Natl Acad Sci U S A* **85**, 1287–1291.

Lancaster B & Adams PR (1986). Calcium-dependent current generating the afterhyperpolarization of hippocampal neurons. *J Neurophysiol* **55**, 1268–1282.

Lancaster B & Batchelor AM (2000). Novel action of BAPTA series chelators on intrinsic K^+ currents in rat hippocampus. *J Physiol* **522**, 231–246.

Lancaster B & Nicoll RA (1987). Properties of two calcium-activated hyperpolarizations in rat hippocampal neurons. *J Physiol* **389**, 187–203.

Ludwig A, Zong X, Jeglitsch M, Hofmann F & Biel M (1998). A family of hyperoplarization-activated mammalian cation channels. *Nature* **393**, 587–591.

Madison DV & Nicoll RA (1982). Noradrenaline blocks accommodation of pyramidal cell discharge in the hippocampus. *Nature* **299**, 636–638.

Madison DV & Nicoll RA (1986*a*). Actions of noradrenaline recorded intracellularly in rat hippocampal CA1 pyramidal neurones *in vitro*. *J Physiol* **372**, 221–244.

Madison DV & Nicoll RA (1986*b*). Cyclic adenosine 3′,5′-monophosphate mediates β-receptor actions of noradrenaline in rat hippocampal pyramidal cells. *J Physiol* **372**, 245–259.

Miller JD, Petrozzino JJ & Connor JA (1995). G protein-coupled receptors mediate a fast excitatory postsynaptic current in CA3 pyramidal neurons in hippocampal slices. *J Neurosci* **15**, 8320–8330.

Muller U & Carew TJ (1998). Serotonin induces temporally and mechanistically distinct phases of persistent PKA activity in *Aplysia* sensory neurons. *Neuron* **21**, 1423–1434.

Nakashima Y & Ono K (1994). Rate-limiting steps in activation of cardiac Cl^- current revealed by photolytic application of cAMP. *Am J Physiol* **267**, H1514–H1522.

Nargeot J, Lester HA, Birdsall NJ, Stockton J, Wassermann NH & Erlanger BF (1982). A photoisomerizable muscarinic agonist. Studies of binding and of conductance relaxations in frog heart. *J General Physiol* **79**, 657–678.

Nerbonne JM, Richard S, Nargeot J & Lester HA (1984). New photoactivatable cyclic nucleotides produce intracellular jumps in cyclic AMP and cyclic GMP concentrations. *Nature* **310**, 74–76.

Nicoll RA (1988). The coupling of neurotransmitter receptors to ion channels in the brain. *Science* **241**, 545–551.

Nicoll RA, Malenka RC & Kauer JA (1990). Functional comparison of neurotransmitter receptor subtypes in mammalian central nervous system. *Physiol Revs* **70**, 513–565.

Øgreid D & Døskeland SO (1981). The kinetics of association of cyclic AMP to the two types of binding sites associated with protein kinase II from bovine myocardium. *FEBS Lett* **129**, 287–292.

Pedarzani P, Krause M, Haug T, Storm JF & Stuhmer W (1998). Modulation of the Ca^{2+}-activated K^+ current sI_{AHP} by a phosphatase-kinase balance under basal conditions in rat CA1 pyramidal neurons. *J Neurophysiol* **79**, 3252–3256.

Pedarzani P & Storm JF (1993). PKA mediates the effects of monoamine transmitters on the K^+ current underlying the slow spike frequency adaptation in hippocampal neurons. *Neuron* **11**, 1023–1035.

Pfrieger FW, Gotmann K & Lux HD (1994). Kinetics of $GABA_B$ receptor-mediated inhibition of calcium currents and excitatory synaptic transmission in hippocampal neurons in vitro. *Neuron* **12**, 97–107.

Rich TC, Fagan KA, Nakata H, Schaack J, Cooper DMF & Karpen JW (2000). Cyclic nucleotide-gated channels colocalize with adenylyl cyclase in regions of restricted cAMP diffusion. *J Gen Physiol* **116**, 147–161.

Rich TC, Fagan KA, Tse TE, Schaack J, Cooper DMF & Karpen JW (2001). A uniform extracellular stimulus triggers distinct cAMP signals in different compartments of a simple cell. *Proc Natl Acad Sci U S A* **98**, 13049–13054.

Richard S, Nerbonne RS, Nargeot J, Lester HA & Garnier D (1985). Photochemically produced intracellular concentration jumps of cAMP mimic the effects of catecholamines on excitation-contraction coupling in frog atrial fibers. *Pflugers Arch* **403**, 312–317.

Santoro B, Grant SGN, Bartsch D & Kandel ER (1997). Interactive cloning with the SH3 domain of N-src identifies a new brain specific ion channel protein, with homology to Eag and cyclic nucleotide-gated channels. *Proc Natl Acad Sci U S A* **94**, 14815–14820.

Savchenko A, Barnes S & Kramer RH (1997). Cyclic-nucleotide-gated channels mediate synaptic feedback by nitric oxide. *Nature* **390**, 694–698.

Stocker M, Krause M & Pedarzani P (1999). An apamin-sensitive Ca^{2+}-activated K^+ current in hippocampal pyramidal neurons. *Proc Natl Acad Sci U S A* **96**, 4662–4667.

Storm JF (1987). Action potential repolarization and a fast after-hyperpolarization in rat hippocampal pyramidal cells. *J Physiol* **385**, 733–759.

Storm JF, Pedarzani P, Haug TM & Winther T (2000). Modulation of K^+ channels in hippocampal neurons: transmitters acting via cyclic AMP enhance the excitability through kinase-dependent and -independent modulation of AHP- and h-channels. In *Slow Synaptic Responses and Modulation*, ed. Kuba K, Higashida H, Brown DA & Yoshioka T, pp. 78–92. Springer-Verlag, Tokyo.

Suaud-Chagny MF, Dugas C, Chergui K, Msghina M & Gonon F (1995). Uptake of dopamine released by impulse flow in the rat mesolimbic and striatal systems in vivo. *J Neurochem* **65**, 2603–2611.

Tanaka H, Clark RB & Giles WR (1996). Positive chronotropic responses of rabbit sino-atrial node cells to flash photolysis of caged isoproterenol and cyclic AMP. *Proc R Soc Lond B* **263**, 241–248.

Westphal RS, Tavalin SJ, Lin JW, Alt NM, Fraser ID, Langeberg LK, Sheng M & Scott JD (1999). Regulation of NMDA receptors by an associated phosphatase-kinase signalling complex. *Science* **285**, 93–96.

Young EC & Krougliak N (2004). Distinct structural determinants of efficacy and sensitivity in the ligand-binding domain of cyclic nucleotide-gated channels. *J Biol Chem* **279**, 3553–3562.

Zaccolo M & Pozzan T (2002). Discrete microdomains with high concentration of cAMP in stimulated rat neonatal cardiac myocytes. *Science* **295**, 1711–1715.

Zagotta WN & Siegelbaum SA (1996). Structure and function of cyclic nucleotide-gated channels. *Ann Rev Neurosci* **19**, 235–263.

Zhong J, Hume JR & Keef KD (1999). Anchoring protein is required for cAMP-dependent stimulation of L-type Ca^{2+} channels in rabbit portal vein. *Am J Physiol* **277**, C840–C844.

Zhou J, Shapiro MS & Hille B (1997). Speed of Ca^{2+} channel modulation by neurotransmitters in rat sympathetic neurons. *J Neurophysiol* **77**, 2040–2048.

Zoli M, Jansson A, Sykova E, Agnati LF & Fuxe K (1999). Volume transmission in the CNS and its relevance for neuropsychopharmacology. *Trends Pharmacol Sci* **20**, 142–150.

Acknowledgements

Financial support was provided by the Sir Jules Thorn Charitable Trust and the Norwegian Research Council (NFR) via the MH, FUGE, EMBIO and Norwegian Centre of Excellence programmes. We would like to thank Kjetil Tasken, University of Oslo for providing and testing the AKAP inhibitory peptide Ht31 and the inactive analogue Ht31P; John Garthwaite and Susan Griffin for assistance with oocyte preparation; Lucia Sivilotti and Steven Broadbent for advice about oocytes and Edgar Young for generous provision of the X-fA4 plasmid.